Atomic dynamics in fluids: Normal mode analysis revisited

Jaeyun Moon* and Lucas Lindsay
Materials Science and Technology Division, Oak Ridge National Laboratory, Oak Ridge, Tennessee 37831, USA

Takeshi Egami
Materials Science and Technology Division, Oak Ridge National Laboratory, Oak Ridge, Tennessee 37831, USA; Department of Materials Science and Engineering, University of Tennessee, Knoxville, Tennessee 37996, USA; and Department of Physics and Astronomy, University of Tennessee, Knoxville, Tennessee 37996, USA

(Received 19 April 2023; accepted 9 June 2023; published 5 July 2023)

Developing microscopic understanding of the thermal properties of liquids is challenging due to their strong dynamic disorder, which prevents characterization of the atomic degrees of freedom. There have been significant research interests in the past few decades to extend the normal mode analysis for solids to instantaneous structures of liquids. However, the nature of normal modes that arise from these unstable structures is still elusive. In this paper, we explore the instantaneous eigenmodes of dynamical matrices of various Lennard-Jones argon liquid and gas systems at high temperatures and show that the normal modes can be interpreted as an interpolation of $T \to \infty$ (gas) and $T = 0$ (solid) mode descriptions. We find that normal modes become increasingly collisional and translational, recovering atomistic gaslike behavior rather than vibrational with increase in temperature, suggesting that normal modes in liquids may be described by both solidlike and gaslike modes.

DOI: 10.1103/PhysRevE.108.014601

I. INTRODUCTION

In contrast to solids and gases, the nature of atomic dynamics of liquids remains elusive due to strong atomic correlations, leading to difficulties in microscopically understanding materials properties of liquids. Among other theoretical approaches that characterize atomic dynamics, normal mode analysis is widely used in various physical [1] and life sciences [2]. In normal mode analysis, one obtains normal mode or eigenmode frequencies and eigenvectors from diagonalization of dynamical matrices built from second derivatives of the interatomic potential of a given structure. Therefore, eigenmode frequencies represent local potential curvatures and eigenvectors depict constituent atomic motions relative to each other.

For solids, normal modes are physically understood as harmonic oscillators about static equilibrium positions, with some exceptions including highly anharmonic systems [3]. These harmonic oscillators are categorized as phonons, propagons, diffusons, and locons based on translational symmetry and mode interaction mechanisms. Normal mode analysis has been successful in describing various thermodynamic and thermal properties of solids, including free energy and heat capacity from a bottom-up perspective [1,4,5]. These properties can now be predicted with high accuracy from routine lattice dynamics calculations [6].

Encouraged by the success in describing vibrational properties of solids, many efforts have been made in recent years to extend the normal mode analysis to liquid systems where instantaneous structure snapshots are used instead of the lattice structure [7–16]. These unstable snapshot structures (nonzero net forces) give rise to modes with imaginary frequencies in addition to modes with real frequencies. As such, a lot of research has been conducted to understand the nature of imaginary modes and various aspects of these have been used to describe some nonequilibrium processes including atomic diffusion [9,17], glass transition [18,19], and melting [20], with varying degrees of success. Despite these efforts, physical understanding of imaginary modes and their relation to various materials properties remains elusive. Real modes in liquids are often interpreted as extrapolation of real modes in solids as harmonic oscillators with well-defined frequencies in a local potential well. However, this assumption becomes particularly questionable at high temperatures as the structures themselves change much faster than most real mode periods. Accurate understanding of the nature of real modes in liquids is, therefore, also lacking.

To build a better understanding of normal mode behaviors, particularly for nonstatic structures (i.e., liquids and gases), we study normal mode characteristics of molecular dynamics (MD) snapshots of various argon systems from solid to gas at extremely high temperatures, up to 10^8 K, at constant volume. In particular, we explore the high temperature limit ($T \to \infty$) of normal modes such that physical interpretations of normal modes at finite, intermediate temperatures can potentially become an interpolation between solid and gas rather than an extrapolation from solid behavior alone. We find that as temperature increases, normal modes involving diatomic units become a dominant feature in the normal mode spectra. Many of these pairs of atoms have positive potential

*Author to whom correspondence should be addressed: moonj@ornl.gov

energies and large kinetic energies such that normal modes with eigenvectors that are parallel with the "bond" can be described as collisional rather than vibrational. Further, we also observe modes progressively being projected to a single atom, mimicking a single atom translating in space. Our findings, therefore, set the scale of the spectrum of eigenmodes of dynamical matrices where in one end we have solidlike vibrational normal modes and in the other end we have gaslike collisional and translational modes.

II. METHODS

Crystalline argon of 1372 atoms in the fcc structure and with a lattice parameter of 5.27 Å was used as the initial input structure for MD simulations using LAMMPS [21] to generate equilibrated atomic structures at various temperatures at constant volume. Interatomic interactions are described by the Lennard-Jones (LJ) potential [22–24]. The parameters used were $\epsilon = 0.0104$ eV and $\sigma = 3.4$ Å. The cutoff distance was 2.5σ and the potential was shifted to eliminate discontinuity. Time steps of 0.1 fs (up to 10^6 K) and 0.01 fs (10^7 K and above) were used. At each temperature, all systems except that of the glass system were equilibrated for 5×10^6 time steps in the canonical ensemble prior to data recording of another 5×10^6 time steps under the same ensemble. The equilibrated atomic structures (snapshots) generated from MD were used to perform lattice dynamics calculations using GULP [25] to obtain eigenfrequencies and eigenvectors of the Γ point dynamical matrices with the entire domain considered as a unit cell. For better statistics, ten such structures at each temperature from MD simulations were used for the lattice dynamics calculations.

Temperatures considered were 1 K for crystal and glass systems and ranging from 10^3 to 10^8 K in increments of factors of 10 for high temperature liquids and gases. In this paper, we consider all systems at 10^6 K and above as gas states as their specific heat is $\frac{3}{2}Nk_B$ within numerical errors where N is the number of atoms. Even though the physical density is kept constant, the effective atomic radius, where the potential energy equals k_BT, thus the effective packing fraction, becomes much reduced at high temperatures, as in gas. Thus, for simplicity, we loosely refer to all other high temperature systems below 10^6 K as liquids. The glass system was created by a standard melt-quench technique (1000 K melting followed by an instantaneous quench to 1 K). This fast cooling rate was required due to typical poor glass formability of monatomic systems. Quenched glass was then equilibrated for 2×10^7 time steps before data recording for 5×10^6 time steps.

To characterize the phases of the various structures, the pair distribution function for each system (shown in Fig. 1) was calculated by

$$g(r) = \frac{1}{4\pi N n r^2} \sum_{i,j} \langle \delta(r - |\boldsymbol{r}_i - \boldsymbol{r}_j|) \rangle \tag{1}$$

where N, n, and $\boldsymbol{r}_i$ are number of atoms, number density, and the atomic position of atom i, respectively. Sharp peaks are observed for the 1 K crystal and broadened peaks and valleys are observed for the 1 K glass demonstrating that short and

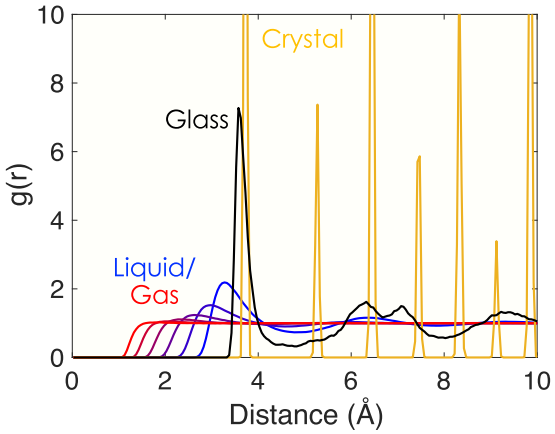

FIG. 1. Pair distribution functions of various argon phases from 1 to 10^8 K under constant volume. The 1 K crystal (yellow curve) has very sharp peaks, some exceeding $g(r) = 30$ (not shown). Broadened peaks and valleys are shown for 1 K glass (black curve) demonstrating short and medium range order. From liquid to gas, progressive disappearance of peaks and valleys is observed with increase in temperature. Temperature ranges are from 10^3 (blue curve) to 10^8 K (red curve) with increments of a factor of 10.

medium range orders are still present in the structure. For the liquid systems, peaks and valleys become broader with increase in temperature and eventually become step functions similar to hard-sphere or dilute gases observed in the literature [26]. The effective diameters of argon atoms decrease with increase in temperature as high kinetic energy enables atoms to approach close to each other, overcoming more of the repulsive portion of the potential, thus mimicking a dilute gas.

From the snapshot structures of all systems, we perform lattice dynamics calculations to obtain eigenmode frequencies (ω_n) and eigenvectors ($\boldsymbol{e}_n$) from Γ point dynamical matrices ($\boldsymbol{D}$) as

$$\omega_n^2 \cdot \boldsymbol{e}_n = \boldsymbol{D} \cdot \boldsymbol{e}_n \tag{2}$$

where subscript n denotes a particular mode from 1 to $3N$ ($N = 1372$ for our systems). Dynamical matrices are related to the potential (U) by

$$D_{\alpha\beta,ij} = \frac{1}{\sqrt{m_i m_j}} \frac{\partial^2 U}{\partial u_{\alpha,i} \partial u_{\beta,j}} \tag{3}$$

where m_i is the mass of atom i and Greek subscripts denote Cartesian directions. There are no phase factors in Eq. (3) as the wave vector under consideration is zero and there are no lattice vectors for our nonperiodic systems. All eigenvectors are real and are orthonormal such that $\boldsymbol{e}_n^T \cdot \boldsymbol{e}_{n'} = \delta_{n,n'}$. As dynamical matrices are Hermitian, all eigenvalues (ω_n^2) are real, while eigenfrequencies (ω_n) can be real or imaginary. We denote imaginary frequencies as negative values in figures below. Overall distributions of available eigenmode populations known as the density of states $g(\omega)$ can then be found by

$$g(\omega) = \sum_{n=1}^{3N} \delta(\omega - \omega_n). \tag{4}$$

Using the mode eigenvectors, we can further characterize each mode by its inverse participation ratio (IPR) and phase quotient (PQ). IPRs (p_n^{-1}) are found by [27]

$$p_n^{-1} = \sum_i \left(\sum_\alpha e^*_{i\alpha,n} e_{i\alpha,n} \right)^2 \tag{5}$$

where $e_{i\alpha,n}$ is the eigenvector component for atom i in direction α for the mode n. IPR gives a measure of how many atoms participate appreciably in the motion of a particular mode; therefore, IPR has been used to qualitatively provide information about the degree of localization of modes for various complex systems [28,29] and even scattering behaviors of acoustic and optic phonons in binary compound crystals [30]. The IPR is conventionally interpreted such that $1/N$ describes all atoms participating in the mode (delocalized) and 1 describes the mode motion completely localized to a single atom.

Phase quotients have also been useful in characterizing normal modes in various materials, especially disordered solids [31–33], and are defined as [31]

$$\mathrm{PQ}_n = \frac{\sum_{i,j\in m} \sum_\alpha e_{i\alpha,n} e_{j\alpha,n}}{\sum_{i,j\in m} \left| \sum_\alpha e_{i\alpha,n} e_{j\alpha,n} \right|} \tag{6}$$

where the sum over m represents counting only the nearest neighbor pairs among atoms i and j. PQ is a measure of the phase relationship of an atom and its neighbors for a given mode. A PQ value of 1 then represents a cluster of atoms all moving in phase, which is the case for Goldstone translational modes, and a PQ value of -1 means that all atoms participating in the mode are moving in the opposite phase or direction with their nearest neighbors. For our systems, we define nearest neighbors to be within $d_c = 2r_c$ where $\frac{4}{3}\pi r_c^3 = \frac{V}{N}$; however, we find that our results are not sensitive to the choice of d_c.

III. RESULTS

A. Normal modes in solids

1. Density of states

Eigenmode densities of states (DOS) for all systems are shown in Fig. 2. Modes with real and imaginary frequencies are plotted on the positive and negative sides of the horizontal axis, respectively. For solids, all modes have real frequencies as shown in Fig. 2(a). Crystalline DOS computed from integration of wave-vector points using the primitive unit cell [one atom per unit cell with primitive lattice vectors: $a_1 = (0.5, 0.5, 0)$, $a_2 = (0, 0.5, 0.5)$, and $a_3 = (0.5, 0, 0.5)$] are also shown as reference. Sharp kinks in the densities of states for crystals are referred to as van Hove singularities where $\frac{d\omega}{dk} = 0$, mostly near zone boundaries [34]. Crystalline argon has three acoustic branches with frequencies ranging up to 2 THz. There are no optical branches due to the primitive unit cell having only one atom. For the rest of the paper, we utilize supercell argon crystal normal modes for analysis for more appropriate comparisons with the other nonperiodic systems of the same size. For the glass system, there are no clear Brillouin zone boundaries or translational symmetry; thus, it has a much broader density of states, though it still has three Goldstone modes with zero frequency. The frequency ranges up to 3 THz, larger than that of crystalline argon likely due to some bonds being shorter than the mean equilibrium bond lengths.

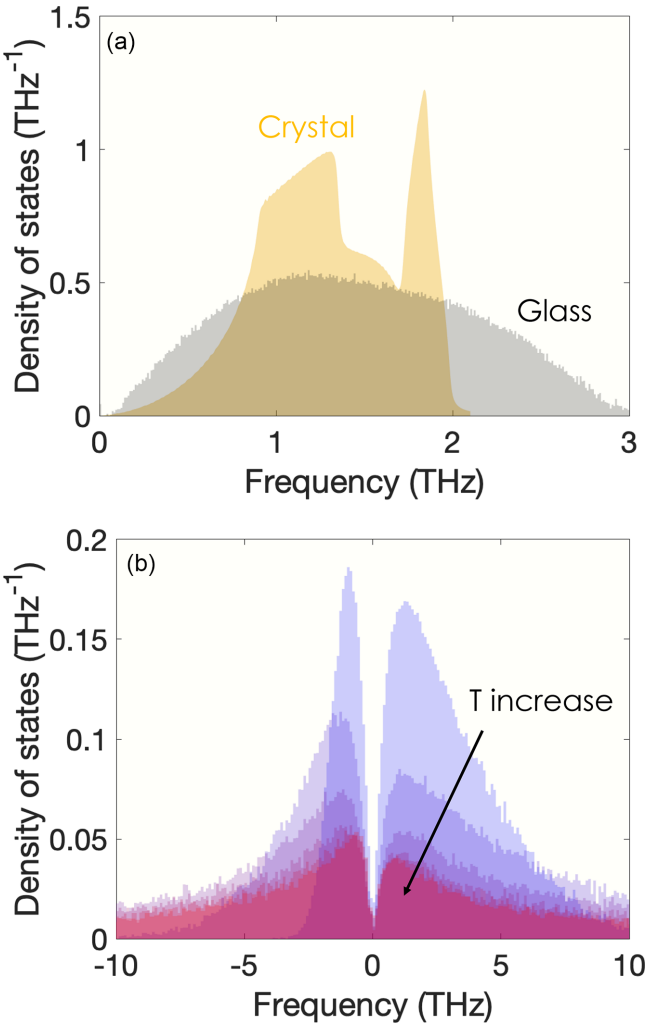

FIG. 2. Densities of states of normal modes for (a) 1 K solids and (b) high temperature liquids and gases from 10^3 K (blue shade) to 10^8 K (red shade) with increments of a factor of 10. Negative frequencies denote imaginary modes. We observe more dominant real modes at low temperatures and increasing importance of imaginary mode populations as measured by the area with increase in temperature. Density of states for glass argon is broadened (black shade) and has a wider frequency range compared to that of crystal argon (orange curve).

2. Inverse participation ratio

Crystalline modes are expected to be spatially delocalized whereas glasses are expected to have some localized modes due to structural disorder. Inverse participation ratios for both are shown in Fig. 3(a) and give a measure of the degree of localization for each mode. In the literature, a normal mode has been considered to be localized when less than 10 to 20% of atoms are participating in the mode motion [32,35,36]. For our purposes here, modes with IPR values over $\mathrm{IPR}_{\mathrm{loc}} = 0.007$ (corresponding to 10% atom participation) are considered to be localized. At 0 THz, we have the Goldstone

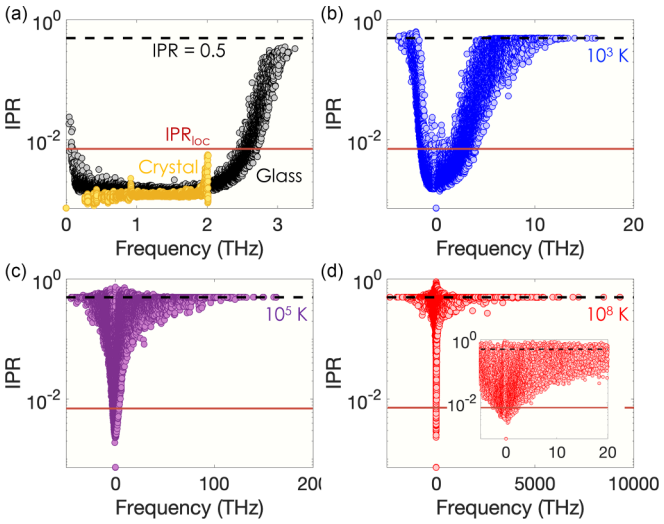

FIG. 3. Inverse participation ratios (measure of localization of modes) for (a) 1 K solids (yellow circles for crystal and black circles for glass) and (b–d) select high temperature liquids and gases at 10^3 K (blue circles), 10^5 K (purple circles), and 10^8 K (red circles). IPR $= 1/N$ corresponds to fully delocalized (all atoms involved), and IPR $= 1$ corresponds to localized to a single atom. Negative frequencies denote imaginary modes. Dashed black line, IPR $= 0.5$ (two-body modes); solid brown line, IPR $=$ IPR$_{loc}$. Modes with IPR $>$ IPR$_{loc}$ are considered to be localized. Inset: The x axis is scaled the same as in panel (b) for comparison.

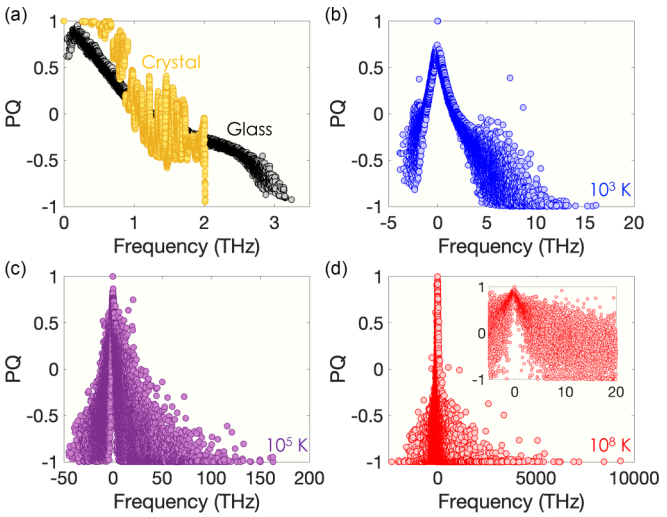

FIG. 4. Phase quotients (measure of motion of atoms compared to neighbors) for (a) 1 K solids (yellow circles for crystal and black circles for glass) and (b–d) select high temperature liquids and gases at 10^3 K (blue circles), 10^5 K (purple circles), and 10^8 K (red circles). PQ $= 1$ corresponds to in phase, while PQ $= -1$ corresponds to out of phase. Negative frequency denotes imaginary modes. Inset: The x axis is scaled the same as in panel (b) for comparison.

modes with IPR $= 1/N$ for both solids where all atoms are participating in the purely translational motion. As expected, all modes for crystalline argon have IPR values less than IPR$_{loc}$, demonstrating that all modes are delocalized. For our glass system, most low frequency modes are also delocalized with some exceptions known as quasilocalized or resonant modes [37–39]. Prior works have proposed that some localization at low frequencies is due to finite size effects [40]. These quasilocalized modes at low frequencies have also been observed in disordered crystals [41,42]. At high frequencies, we observe a significant number of modes with IPR values greater than IPR$_{loc}$, similar to that observed previously in another single element glass (amorphous silicon) [32]. These localized vibrational modes, often referred to as locons in the glass literature, form a small fraction of the total number of modes, about 2 to 3%. Locons typically have low thermal diffusivities and conductivities compared to extended modes [32,43,44]. Maximum IPR values found in our glass system are around 0.3.

3. Phase quotient

Modal PQs for our solid argon systems that characterize relative mode motion of an atom with its neighbors are shown in Fig. 4(a) (PQ $= 1$ for fully in phase and PQ $= -1$ for fully out of phase). For the crystal system, some modes, including the 0 THz Goldstone modes, have PQ $= 1$ at low frequencies demonstrating that atoms are moving nearly in phase with their neighbors. With increase in frequency, PQ decreases and eventually appears to fluctuate between PQ $= 0$ and -0.5 and approaches PQ ≈ -1. While crystalline argon does not have optical modes (typical out-of-phase vibrations in compound crystals), away from 0 THz acoustic modes develop phase differences among neighboring atoms, which underlies the decrease in PQ values. For the argon glass, we observe a monotonic decrease in PQ values with increase in frequency away from 0 THz Goldstone modes that have PQ $= 1$, similar to other glasses reported in the literature [32,33]. The lowest PQ values found in the glass system are around -0.9, close to the fully out-of-phase value of PQ $= -1$. Prior works utilizing PQs in glasses have proposed that modes with PQ > 0 and PQ < 0 represent acoustic-like and optical-like modes, respectively [32,33]. Using this notation, an acoustic- to optical-like mode transition occurs around 1.2 THz for argon glass.

With this normal mode analysis for solids as background context, we next characterize normal modes in the same way for various liquid and gas systems at higher temperatures.

B. Normal modes in liquids and gases

1. Density of states

Normal mode densities of states for all liquid and gas systems are shown in Fig. 2(b). Similar to the solids, densities of states are scaled such that the area under the curve is 1. Only the low frequency region $|\omega| < 10$ THz is shown for ease of comparisons. Perhaps, the most notable difference in the normal mode densities of states of liquids and gases compared to those of solids is the significant presence of imaginary modes. We see a clear temperature dependence: the imaginary part of the spectra becomes more prominent with increase in temperature as measured by the area. However, as noted previously [45], the rate at which this happens slows down at high temperatures as demonstrated in Fig. 2(b). We have previously proposed that an equal number of imaginary modes and real modes marks a transition to a gaslike phase [45]. With

increase in temperature, also the frequency ranges increase significantly up to 10^4 THz and down to -2500 THz ($i\omega$) for the 10^8 K gas but with very small probability.

Following Zwanzig's approach to relate self-diffusion coefficients to normal modes [46], some prior works have tried to express the self-diffusion coefficient with the fractions of imaginary modes and real modes over all modes [9,10,12,20,47]. Some other works have tried to relate normal modes in nonsolids to their specific heats [45,48] and glass transitions [18,19]. Extrapolating the physical interpretation of real modes in solids to nonsolids, it is often assumed that for real modes, liquid atoms vibrate as harmonic oscillators within a local potential well determined from the cage of nearest neighbor atoms [14,20,48]. However, physical interpretation of both real and imaginary modes in liquids is not clear and motivated this paper.

We aim below to characterize the high temperature limit of eigenmodes of dynamical matrices ($T \to \infty$) under the same density as those of solids such that interpretation of eigenmodes of liquids may potentially become an interpolation from both $T = 0$ and $T \to \infty$ eigenmodes rather than an extrapolation only from the $T = 0$ crystalline modes that we are familiar with.

2. *Inverse participation ratio*

Similar to solids, we characterize eigenmodes of liquids and gases via inverse participation ratios and phase quotients. Inverse participation ratio spectra at select high temperatures (10^3, 10^5, and 10^8 K) are shown in Figs. 3(b)–3(d). At 10^3 K, we see an asymmetric U shape with high real and imaginary frequency modes being strongly localized and low frequency modes being more extended. This IPR behavior mimics the glass spectral features, although the liquid system has a large component of imaginary modes. Similar trends have been previously shown in other liquid systems [17]. In the limit of high frequency, we seem to approach IPR = 0.5. With increase in temperature, low frequency modes have higher IPR values, filling up the empty region in the U shapes found at low temperatures. For our highest temperature system, we have a crosslike shape with the vertical limits dictated by the lowest IPR ($1/N$) from the pure translational modes and highest IPR approaching ≈0.9 and with high frequency modes having IPRs exactly equal to 0.5. At 10^8 K, nearly all modes (over 98% of the mode populations) are "localized" in the conventional interpretation having IPR > IPR_{loc}.

3. *Phase quotient*

Phase quotients for liquids and gases are shown in Figs. 4(b)–4(d). For all systems, the phase quotient spectra appear nearly symmetric for real and imaginary modes with the exception of the long tail in the real frequency spectrum. A monotonic decrease in PQs is apparent moving away from 0 THz, similar to the glass system. One notable trend observed for liquids and gases vs solids is the increasing presence of modes with PQ = −1 with increase in temperature. In both metrics (IPR and PQ), we do not observe distinct differences between real mode and imaginary mode characters.

Examining the gas modes more closely, we find some modes with exact values of IPR = 0.5 and/or PQ = −1, modes that are absent in the solid systems. Bivariate probability distributions of the IPRs and PQs for argon at select temperatures are plotted in Fig. 5 and demonstrate a strong trend: going from solids to gases, modes with both IPR = 0.5 and PQ = −1 become the dominant population. In the limit that $T \to \infty$, we imagine that this trend continues as atoms become effectively smaller and this character will govern the normal mode spectra. We have done additional calculations for 864 and 4000 atom domain sizes and observed no clear size effect on mode characters as shown in Fig. 9 in Appendix. As our interest lies in using normal mode analysis to understand liquids in terms of higher T gas phases, we aim to fully understand these modes.

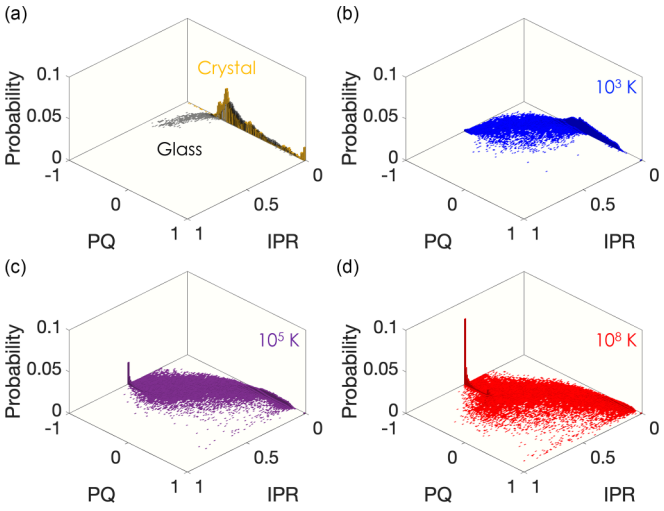

FIG. 5. Bivariate (inverse participation ratio and phase quotient) probability distributions for (a) 1 K solids (yellow for crystal and black for glass) and (b–d) select high temperature liquids and gases at 10^3 K (blue), 10^5 K (purple), and 10^8 K (red). We observe a peak appearing at IPR = 0.5 and PQ = −1 with increase in temperature.

4. *IPR = 0.5 and PQ = −1 modes*

IPR of 0.5 indicates that two atoms are participating in the mode and PQ = −1 describes eigenvectors among neighboring atoms that are fully out of phase. From the simulations we have identified pairs of atoms that govern modes with IPR = 0.5 and PQ = −1 and examined the roles of these atoms in all modes of the system. As a representative example, Fig. 6(a) gives (x-direction) eigenvector components for such a pair (atom 1, blue; atom 2, red) for all modes at 10^8 K. This pair of atoms contributes negligibly to most modes (near zero amplitudes) as nearly all modes are localized to other atoms (large IPR values). However, for modes with finite and sometimes large x components (see inset) for this pair, the eigenmotions of the two atoms are the same (overlapping components), while three modes have identical amplitudes in opposite direction. Thus, of the multitudes of other mode motions, their relative motions are defined by three modes with opposite directions (IPR = 0.5 and PQ = −1). y and z eigenvector components have similar features (not shown to avoid redundancy).

Interestingly, the three modes that govern the motion of the pairs of atoms with IPR = 0.5 and PQ = −1 can be

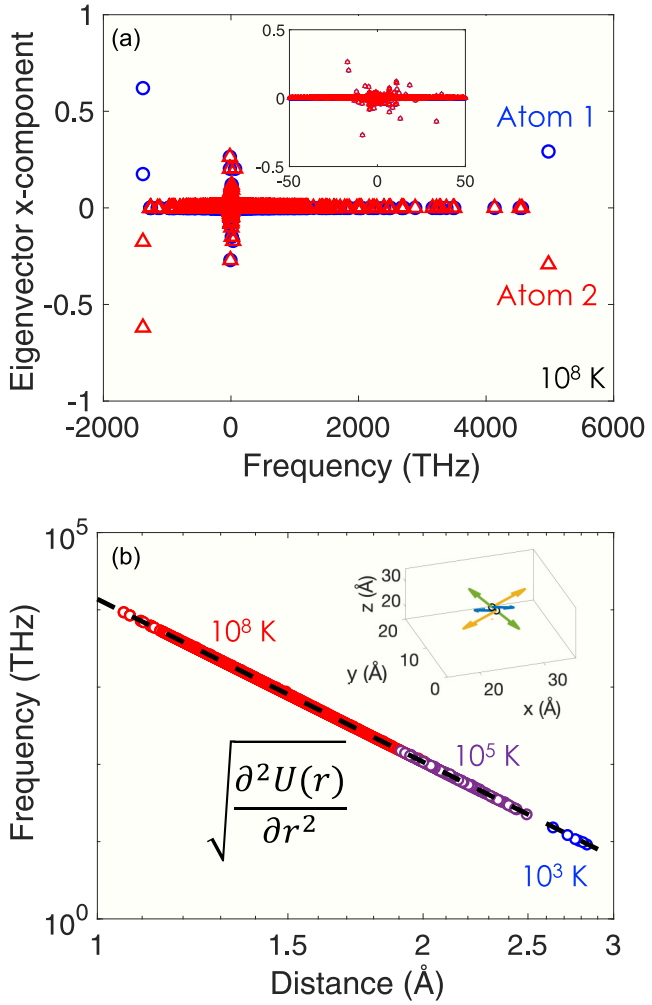

FIG. 6. (a) Eigenvector components (x direction for a pair of atoms identified to have IPR $= 0.5$ and PQ $= -1$) for all modes at 10^8 K. Blue and red colors represent atom 1 and atom 2 in the pair, respectively. Inset: Zoomed-in view near 0 THz. All eigenvectors are in phase between the two atoms except three which are fully out of phase. All pairs of atoms with these features are identified and their along-the-bond mode (green arrows in inset) frequencies and their distances are shown in panel (b). A clear relation to the LJ pair potential (black dashed line) is demonstrated.

decomposed into one real mode and two imaginary modes. Visualization of these three modes projected on a pair of atoms is representatively shown in the inset of Fig. 6(b). The real modes have eigenvectors along the "bond" (green arrows), while atomic motion for the other two imaginary modes is orthogonal to the bond. In essence, the repulsive force along the bond directs the atoms to a more stable position while there is no energy loss in the motion of the other two modes, similar to rotational modes.

In bulk dense solids, each atom sits in an effective potential that is the summation of all neighboring interatomic potential interactions. However, for the pairs of atoms dominating the eigenmotions for IPR $= 0.5$ and PQ $= -1$ modes, the behavior is simulating independent two-atom motion governed by a single pair potential $[U_{i,j}(r)]$ that defines the mode frequencies, while other interactions are negligible. This leads to three Goldstone modes (two atoms moving in phase for three Cartesian degrees of freedom) and three out-of-phase modes with opposite eigenvector directions with one being along the bond. Mode frequency along the bond is strictly determined by $\frac{\partial^2 U_{i,j}(r)}{\partial r^2}$. Along-the-bond mode frequencies with IPR $= 0.5$ and PQ $= -1$ as a function of distance between the atomic pairs are shown in Fig. 6(b) for both liquid and gas systems. The nearly perfect power law behavior ($\sim r^{-7}$) demonstrates that these mode frequencies are purely determined by the second derivative of the pair potential, similar to truly independent two-atom interactions. We also observe that there is a temperature dependence in the bond distance and mode frequencies. There is a large distribution of bond lengths and frequencies at high temperatures while the distribution is smaller for low temperatures. While dynamical matrices are built based purely on the potential of a static structure, kinetic energies play a dominant role in determining the atomic locations that feed into the dynamical matrices, especially at high temperatures (liquids and gases). The larger the kinetic energies that atoms have, the closer they can approach each other, leading to higher frequencies for these modes.

5. *Collisons*

Normal modes are typically used to describe phonon quasiparticles or harmonic oscillators in solids. Even in gases, there can be internal degrees of freedom for nonmonoatomic species that lead to vibrations (e.g., H_2 and O_2). However, the results described above show that along-the-bond modes with IPR $= 0.5$ and PQ $= -1$ should be considered as collisional rather than vibrational. Even with absence of kinetic energy, if pairs of argon atoms are initially placed at distances shown in Fig. 6(b) and their motions are allowed to evolve with time, their potential energy is positive $[U_{\mathrm{LJ}}(r < 3.4\ \text{Å}) > 0]$ such that they dissociate after participating in the along-the-bond mode motion with kinetic energies determined by energy conservation. We, thereby, characterize these modes as two-body collisional modes or "collisons."

6. *Translatons*

As evident from Fig. 3, the highest IPR values which are located near 0 THz also depend on temperature. Traditional interpretation of IPRs that IPR is a measure of the number of atoms participating in the mode does not strictly work here as there are many IPRs between $\frac{1}{2}$ (two atoms participating) and 1 (one atom participating). However, we find that these high IPR modes appear to have concentrated eigenvector amplitude on a single atom as demonstrated in Fig. 7.

It is, therefore, expected that under different conditions there exist modes with IPR approaching 1 where mode motion is projected to a single atom translating through space with small frequency. This is consistent with what we know about dilute gas eigenmodes where nearly all modes have zero eigenfrequencies due to small potential interactions. As we progressively reach lower densities, atomic interactions will become less frequent and more uninterrupted translational motion will appear, which would have approximately zero eigenfrequency. In the same token, in the limit of $T \to \infty$ where atoms become point particlelike and overall collisions become less frequent, we would expect modes that purely

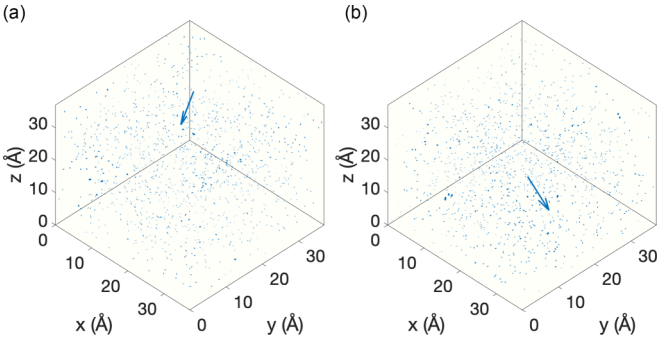

FIG. 7. All eigenvector maps of all atoms for (a) −0.3 THz mode with IPR = 0.82 and (b) 0.1 THz mode with IPR = 0.74, among the highest IPRs for 10^8 K systems. All eigenvector amplitudes are multiplied by a factor of 10 for easier visualization, same as Fig. 6(b). We observe that for these modes eigenvector magnitudes are concentrated to a single atom.

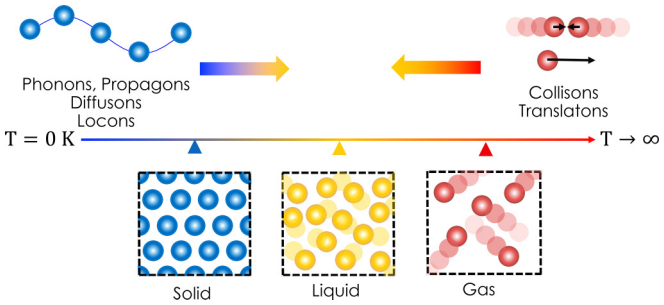

FIG. 8. Spectrum of eigenmodes of dynamical matrices from $T = 0$ K to $T \to \infty$ under constant volume. At the $T = 0$ limit, we have vibrational modes (phonons, propagons, diffusons, and locons depending on disorder and localization). At the high temperature limit, both real and imaginary modes are expected to be gaslike, which we characterize as collisons and translatons. Eigenmodes for finite, intermediate temperature structures could potentially be described through these two limits.

describe translational motion, or what we may characterize as "translatons," to appear. We have done 10^{12} K IPR calculations (not shown) and found that IPR approaches as high as 0.97 vs 0.85 observed in our 10^8 K system.

IV. CONCLUDING REMARKS

Our results on the normal mode analysis on heat capacities [45], pair distribution functions, and mode characters by IPRs and PQs suggest that in the limit of $T \to \infty$, particles will effectively behave as point particles and two-body collisional modes dominate the particle dynamics, even when the volume is kept constant at that of a solid. This is consistent with real gas collisions where two-atom collisions become statistically dominant with increase in temperature over many-body collisions [49]. In glasses, eigenmodes are vibrational within a local harmonic well and have been categorized into propagons, diffusons, and locons depending on the degree of localization [32,50]. Although there exist different ways to categorize these modes [35,43,51], they often rely on the normal mode analysis, i.e., eigenvector characters. Similarly, we categorize eigenmodes at $T \to \infty$ into collisons and translatons from their eigenvector characters and their local atomic environment.

With these insights into the behavior of high temperature (gas) eigenmodes of dynamical matrices coupled with the vast body of research regarding $T = 0$ eigenmodes (solid), we propose that eigenmodes in liquids may be best considered as a collection of both solidlike vibrational and gaslike collisional and translational modes as summarized in Fig. 8. While the probability of having two-body collisional modes decreases with decreasing temperature, we still observe these modes even in the lowest temperature liquid argon considered here. In real liquids, the evaporation behavior strongly depends on pressure. To avoid such complications we chose a well-defined case of constant volume. To confirm the generality of the approach, we have done normal mode characterizations of LJ argon under 1 bar (NPT) and found consistent results as with the current system examined in our paper. In this paper, a simple Lennard-Jones pair potential was used throughout. We expect that our high temperature limit results will not depend on the choice of interatomic potential (two-body, many-body, etc.) as all systems will become an atomic gas where details of the nature of the interactions become less important. While our results are based on a single element system (LJ argon), gaslike modes, collisons and translatons, would also appear in multi-element systems (for example, molecules colliding with other molecules).

In this paper, we explored the high temperature limits of eigenmodes of dynamical matrices through the lens of inverse participation ratios and phase quotients in the context of $T \sim 0$ K eigenmodes. In crystals and glasses, normal modes are considered to be vibrational in nature with most being delocalized in space. With increase in temperature we find that an increasing number of eigenmodes become gaslike collisional and translational modes. Our paper, therefore, sets the scale of spectra of different eigenmodes such that normal modes of liquids can be described in terms of evolving characters, rather than extrapolation from our understanding of normal modes in solids alone as often done in literature.

ACKNOWLEDGMENTS

The authors thank Simon Thébaud for helpful discussions on the nature of normal modes. This research was supported by the U.S. Department of Energy, Office of Science, Basic Energy Sciences, Materials Sciences and Engineering Division. This work used the Extreme Science and Engineering Discovery Environment Expanse under Allocation No. TG-MAT200012. This research used resources of the National Energy Research Scientific Computing Center (NERSC), a U.S. Department of Energy Office of Science User Facility located at Lawrence Berkeley National Laboratory, operated under Contract No. DE-AC02-05CH11231 using NERSC Grant No. BES-ERCAPERCAP0020503.

APPENDIX: SIZE EFFECTS IN MODE CHARACTERS

In addition to our 1372 atom domain cell discussed in the main text, we have calculated inverse participation ratios and

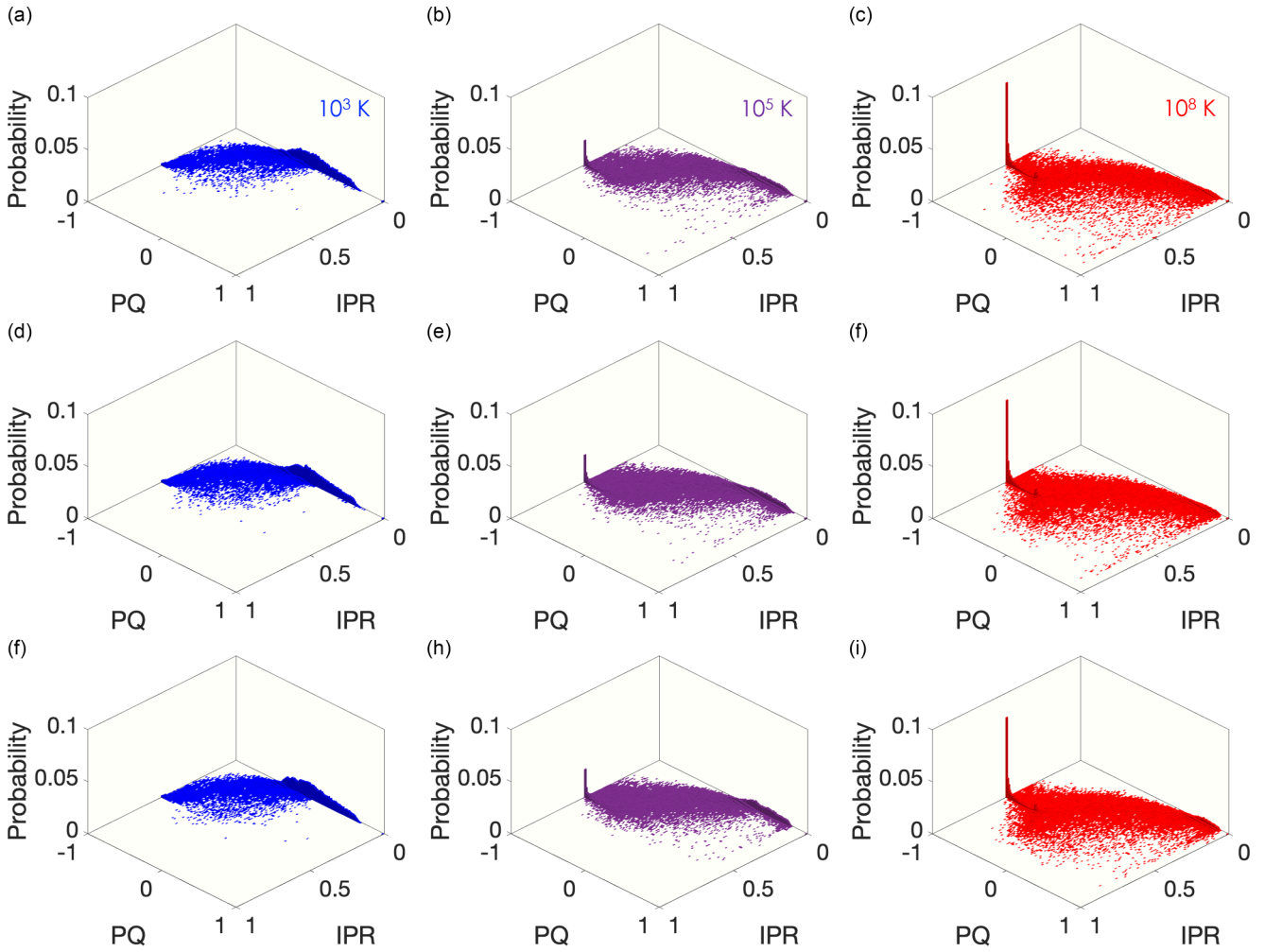

FIG. 9. Bivariate (inverse participation ratio and phase quotient) probability distributions for [(a)–(c)] 864, [(d), (e)] 1372, and [(g)–(i)] 4000 atom domain cells at 10^3 K (blue), 10^5 K (purple), and 10^8 K (red). We observe no clear size dependence in mode characters.

phase quotients for 864 atom and 4000 atom domains using the same simulation procedures as our 1372 atom domain calculations. As demonstrated in Fig. 9, no clear size dependence in the normal mode characters is observed.

[1] M. T. Dove, *Introduction to Lattice Dynamics* (Cambridge University, New York, 1993), Vol. 4.

[2] D. A. Case, Normal mode analysis of protein dynamics, Curr. Opin. Struct. Biol. **4**, 285 (1994).

[3] B. Sun, S. Niu, R. P. Hermann, J. Moon, N. Shulumba, K. Page, B. Zhao, A. S. Thind, K. Mahalingam, J. Milam-Guerrero, R. Haiges, M. Mecklenburg, B. C. Melot, Y.-D. Jho, B. M. Howe, R. Mishra, A. Alatas, B. Winn, M. E. Manley, J. Ravichandran *et al.*, High frequency atomic tunneling yields ultralow and glass-like thermal conductivity in chalcogenide single crystals, Nat. Commun. **11**, 6039 (2020).

[4] L. Lindsay, C. Hua, X. L. Ruan, and S. Lee, Survey of ab initio phonon thermal transport, Mater. Today Phys. **7**, 106 (2018).

[5] A. J. H. McGaughey, A. Jain, H.-Y. Kim, and B. Fu, Phonon properties and thermal conductivity from first principles, lattice dynamics, and the Boltzmann transport equation, J. Appl. Phys. **125**, 011101 (2019).

[6] A. Togo and I. Tanaka, First principles phonon calculations in materials science, Scr. Mater. **108**, 1 (2015).

[7] M. Cho, G. R. Fleming, S. Saito, I. Ohmine, and R. M. Stratt, Instantaneous normal mode analysis of liquid water, J. Chem. Phys. **100**, 6672 (1994).

[8] T. Keyes, Instantaneous normal mode approach to liquid state dynamics, J. Phys. Chem. A **101**, 2921 (1997).

[9] G. Seeley, T. Keyes, and B. Madan, Isobaric diffusion constants in simple liquids and normal mode analysis, J. Chem. Phys. **95**, 3847 (1991).

[10] G. Seeley and T. Keyes, Normal mode analysis of liquid-state dynamics, J. Chem. Phys. **91**, 5581 (1989).

[11] J. D. Gezelter, E. Rabani, and B. J. Berne, Can imaginary instantaneous normal mode frequencies predict barriers to self-diffusion? J. Chem. Phys. **107**, 4618 (1997).

[12] V. I. Clapa, T. Kottos, and F. W. Starr, Localization transition of instantaneous normal modes and liquid diffusion, J. Chem. Phys. **136**, 144504 (2012).

[13] W. Schirmacher, T. Bryk, and G. Ruocco, Modeling the instantaneous normal mode spectra of liquids as that of unstable elastic media, Proc. Natl. Acad. Sci. USA **119**, e2119288119 (2022).
[14] A. Zaccone and M. Baggioli, Universal law for the vibrational density of states of liquids, Proc. Natl. Acad. Sci. USA **118**, e2022303118 (2021).
[15] R. M. Stratt, The instantaneous normal modes of liquids, Acc. Chem. Res. **28**, 201 (1995).
[16] S. Mossa, T. Bryk, G. Ruocco, and W. Schirmacher, Instantaneous normal modes in liquids: A heterogeneous-elastic-medium approach, arXiv:2302.02681.
[17] W. Zhang, J. F. Douglas, and F. W. Starr, What does the instantaneous normal mode spectrum tell us about dynamical heterogeneity in glass-forming fluids? J. Chem. Phys. **151**, 184904 (2019).
[18] S. D. Bembenek and B. B. Laird, Instantaneous Normal Modes and the Glass Transition, Phys. Rev. Lett. **74**, 936 (1995).
[19] S. D. Bembenek and B. B. Laird, Instantaneous normal modes analysis of amorphous and supercooled silica, J. Chem. Phys. **114**, 2340 (2001).
[20] A. Melzer, A. Schella, J. Schablinski, D. Block, and A. Piel, Instantaneous Normal Mode Analysis of Melting of Finite Dust Clusters, Phys. Rev. Lett. **108**, 225001 (2012).
[21] S. Plimpton, Fast parallel algorithms for short-range molecular dynamics, J. Comput. Phys. **117**, 1 (1995).
[22] J. E. Jones, On the determination of molecular fields. II. From the equation of state of a gas, Proc. R. Soc. A **106**, 463 (1924).
[23] J. E. Jones, On the determination of molecular fields. I. From the variation of the viscosity of a gas with temperature, Proc. R. Soc. A **106**, 441 (1924).
[24] A. Rahman, M. J. Mandell, and J. P. McTague, Molecular dynamics study of an amorphous Lennard-Jones system at low temperature, J. Chem. Phys. **64**, 1564 (1976).
[25] J. D. Gale, GULP: A computer program for the symmetry-adapted simulation of solids, J. Chem. Soc., Faraday Trans. **93**, 629 (1997).
[26] D. A. McQuarrie, *Statistical Mechanics* (Sterling, Sausalito, California, 2000).
[27] R. J. Bell and P. Dean, Atomic vibrations in vitreous silica, Discuss. Faraday Soc. **50**, 55 (1970).
[28] J. Moon and A. J. Minnich, Sub-amorphous thermal conductivity in amorphous heterogeneous nanocomposites, RSC Adv. **6**, 105154 (2016).
[29] F. DeAngelis, M. G. Muraleedharan, J. Moon, H. R. Seyf, A. J. Minnich, A. J. H. McGaughey, and A. Henry, Thermal transport in disordered materials, Nanoscale Microscale Thermophys. Eng. **23**, 81 (2018).
[30] L. Lindsay, D. A. Broido, and T. L. Reinecke, Phonon-isotope scattering and thermal conductivity in materials with a large isotope effect: A first-principles study, Phys. Rev. B **88**, 144306 (2013).
[31] R. J. Bell and D. C. Hibbins-Butler, Acoustic and optical modes in vitreous silica, germania and beryllium fluoride, J. Phys. C **8**, 787 (1975).
[32] P. B. Allen, J. L. Feldman, J. Fabian, and F. Wooten, Diffusons, locons and propagons: Character of atomie yibrations in amorphous Si, Philos. Mag. B **79**, 1715 (1999).
[33] H. R. Seyf, W. Lv, A. Rohskopf, and A. Henry, The Importance of Phonons with Negative Phase Quotient in Disordered Solids, Sci. Rep. **8**, 2627 (2018).
[34] C. Kittel, Introduction to Solid State Physics, 5th ed. (John Wiley & Sons, Inc, New York, 1976).
[35] H. R. Seyf and A. Henry, A method for distinguishing between propagons, diffusions, and locons, J. Appl. Phys. **120**, 025101 (2016).
[36] K. Aryana, D. A. Stewart, J. T. Gaskins, J. Nag, J. C. Read, D. H. Olson, M. K. Grobis, and P. E. Hopkins, Tuning network topology and vibrational mode localization to achieve ultralow thermal conductivity in amorphous chalcogenides, Nat. Commun. **12**, 2817 (2021).
[37] E. Lerner, G. Düring, and E. Bouchbinder, Statistics and Properties of Low-Frequency Vibrational Modes in Structural Glasses, Phys. Rev. Lett. **117**, 035501 (2016).
[38] H. Mizuno, H. Shiba, and A. Ikeda, Continuum limit of the vibrational properties of amorphous solids, Proc. Natl. Acad. Sci. USA **114**, E9767 (2017).
[39] N. S. Shcheblanov, M. E. Povarnitsyn, J. D. Wiles, S. R. Elliott, and S. N. Taraskin, Quasilocalized vibrations in vitreous silica, Phys. Status Solidi B **258**, 2000422 (2021).
[40] J. L. Feldman, P. B. Allen, and S. R. Bickham, Numerical study of low-frequency vibrations in amorphous silicon, Phys. Rev. B **59**, 3551 (1999).
[41] H. Mizuno, S. Mossa, and J.-L. Barrat, Elastic heterogeneity, vibrational states, and thermal conductivity across an amorphisation transition, Europhys. Lett. **104**, 56001 (2013).
[42] E. Lerner and E. Bouchbinder, Disordered Crystals Reveal Soft Quasilocalized Glassy Excitations, Phys. Rev. Lett. **129**, 095501 (2022).
[43] J. Moon, B. Latour, and A. J. Minnich, Propagating elastic vibrations dominate thermal conduction in amorphous silicon, Phys. Rev. B **97**, 024201 (2018).
[44] T. Kim, J. Moon, and A. J. Minnich, Origin of micrometer-scale propagation lengths of heat-carrying acoustic excitations in amorphous silicon, Phys. Rev. Mater. **5**, 065602 (2021).
[45] J. Moon, S. Thébaud, L. Lindsay, and T. Egami, Microscopic view of heat capacity of matter: solid, liquid, and gas, arXiv:2210.06218.
[46] R. Zwanzig, On the relation between self-diffusion and viscosity of liquids, J. Chem. Phys. **79**, 4507 (1983).
[47] E. L. Nave, A. Scala, F. W. Starr, F. Sciortino, and H. E. Stanley, Instantaneous Normal Mode Analysis of Supercooled Water, Phys. Rev. Lett. **84**, 4605 (2000).
[48] M. Baggioli and A. Zaccone, Explaining the specific heat of liquids based on instantaneous normal modes, Phys. Rev. E **104**, 014103 (2021).
[49] A. Bonasera and F. Gulminelli, Competition between two- and three-body collisions in a dense gas at finite temperature, Phys. Lett. B **259**, 399 (1991).
[50] P. B. Allen and J. L. Feldman, Thermal Conductivity of Glasses: Theory and Application to Amorphous Si, Phys. Rev. Lett. **62**, 645 (1989).
[51] J. Moon, Examining normal modes as fundamental heat carriers in amorphous solids: The case of amorphous silicon, J. Appl. Phys. **130**, 055101 (2021).